Applied Thermal Engineering 280 (2025) 128130

Contents lists available at ScienceDirect

Applied Thermal Engineering

journal homepage: www.elsevier.com/locate/apthermeng

Research Paper

A novel 3D-CFD-simulation-based model to predict potential boiling-related erosion damage in engine cooling circuits

Pietro Pigani [a], Fabio Berni [a,*], Giovanni Paini [b], Roberto Tonelli [b], Stefano Fontanesi [a]

[a] Università Degli Studi di Modena e Reggio Emilia, Italy
[b] Ferrari S.p.A, Italy

ARTICLE INFO

Keywords:
Boiling
Erosion
Failure
Bubble collapse
Cooling circuit
3D-CFD

ABSTRACT

In recent years, the increasing power density of reciprocating internal combustion engines has posed significant challenges to maintain optimal temperature conditions and to preserve thermo-mechanical reliability. In order to improve the cooling circuit performance, local nucleate boiling has become a key phenomenon to promote pointwise heat transfer. However, experimental studies also revealed that, in presence of boiling, surface erosion can potentially occur in specific areas of the engine (especially the head), based on operating conditions and geometry of the cooling circuit. In this context, the development of a dedicated tool able to accurately predict the occurrence of boiling-induced erosion is essential to optimize design and thermal management of the engine, in order to mitigate the onset of potential severe damages.

A 3D-CFD tool to predict damage in cooling circuits is proposed in the present work and it relies on both a conjugate heat transfer model of the engine and a novel purposely developed parameter. As for the former, it provides a detailed description of the engine and it is characterized by an accurate modelling of the boiling phenomenon. As for the latter, despite the availability of numerous erosion models in the context of cavitation, no reliable or widely accepted tool currently exists for predicting material surface erosion caused by the collapse of vapor bubbles in presence of boiling. In the paper, a model is proposed, based on the latest research findings available in literature on the vapor bubble condensation process. The model is synthetized by a novel erosion parameter, which accounts for key factors influencing the bubble collapse phenomenon, including vapor fraction, liquid subcooling level, thermal gradient and local velocity field. The higher the erosion parameter is, the higher the risk of severe damage results.

The CFD tool is validated against experimental data on two different high-performance engines. The CHT model thermal field is compared to temperatures from thermocouples installed at the test bench. The predicted regions of potential boiling-induced damage, indicated by peaks of erosion parameter distribution, exhibit strong correlation with the experimental images showing the regions of severe damage.

Interestingly, although the erosion parameter is developed to investigate damage in high-performance current-production reciprocating internal combustion engines, it can be applied, in principle, to any engine or cooling circuit. In addition, the implementation is straightforward as it is just a post-processing tool. Therefore, it can be applied to elaborate the results of any existing simulation.

1. Introduction

Modern high-performance reciprocating internal combustion engines continuously undergo a rise in specific power, thus making their thermal management an increasingly complex challenge. In fact, the cooling system has to dissipate higher and higher heat fluxes, and the temperature of the metal surface in contact with the coolant often exceeds the saturation temperature of the fluid, leading to nucleate boiling onset. Actually, if properly controlled, boiling can be strongly beneficial, as it enhances the heat transfer efficiency by increasing the amount of heat removed, thus optimizing the overall cooling system performance.

However, boiling is a complex phenomenon not easy to handle. Experimental evidence reveals that it can lead to surface erosion of the cooling circuit. For instance, in [1], it is shown that in specific areas of the engine head erosion can be noticed, as a consequence of high temperatures that lead to massive bubble formation.

Research on erosion due to boiling in cooling circuits has seldom

* Corresponding author.
E-mail address: fabio.berni@unimore.it (F. Berni).

https://doi.org/10.1016/j.applthermaleng.2025.128130
Received 11 June 2025; Received in revised form 4 August 2025; Accepted 30 August 2025
Available online 1 September 2025

Nomenclature

Symbols/Acronyms

BMEP	Brake mean effective pressure
CFD	Computational fluid dynamics
CHT	Conjugate heat transfer
EMP	Eulerian multi-phase
GEP	GruMo erosion parameter
max	Maximum
min	Minimum
VOF	Volume Of fluid
WOT	Wide open throttle
B	Bore
S	Stroke
α_v	Vapor volume fraction
γ	Dimensionless wall distance (i.e. ratio between wall distance and radius of the bubble)
C_{ew}	Boiling model constant
C_μ	Turbulence model constant
c_{p_l}	Specific heat of the liquid
C_{qw}	Boiling model constant
ΔT_{sub}	Subcooling level
ε	Turbulent kinetic energy dissipation rate
g	Gravitational acceleration
h_{lat}	Enthalpy of vaporization
k	Turbulent kinetic energy
μ_l	Liquid dynamic viscosity
$\dot{m}_{ew}$	Vapor production rate
n_p	Boiling model constant
P_g	Gauge pressure
Pr_l	Prandtl number of the liquid
q_{bw}	Heat flux increment due to boiling
q_{conv}	Convective heat flux
q_{TOT}	Total heat flux
Re	Reynolds number
ρ_l	Liquid density
ρ_v	Vapor density
σ	Surface tension
Σ	Sum
t	Time
T_{cell}	Cell temperature
T_{CFD}	Temperature by CFD
T_{EXP}	Temperature by experiments
T_{liquid}	Temperature of liquid phase
T_{sat}	Saturation temperature
T_{vapor}	Temperature of vapor phase
T_{wall}	Wall temperature
U	Velocity Magnitude
u_τ	Friction velocity
V_{dam}	Damaged volume
V_{shear}	Shear flow velocity (i.e. velocity of the flow with respect to the wall)
y^+	Dimensionless wall distance
$\vec{\nabla}(T)$	Temperature gradient
$\vec{\nabla}(T)_{//wall}$	Wall-parallel component of the temperature gradient
$\vec{\nabla}(T)_{\perp wall}$	Wall-normal component of the temperature gradient

been carried out. In industrial applications, erosive phenomena are typically associated to cavitation, which refers to the generation and collapse of vapor cavities or bubbles in a liquid, due to local pressure fluctuations resulting from high speed flow or vibration. Cavitation is typically encountered in applications such as marine propellers [2], pumps [3], hydraulic turbines [4] and injectors [5]. Cavitation-induced erosion has also been observed in engine cooling circuits, but in areas in contact with the cylinder liner. In fact, in the coolant galleries pertaining to this region, pressure fluctuations are induced by the tilting of the liner walls during the engine cycle. These fluctuations lead to the formation of microscopic vapor bubbles, which subsequently collapse violently, potentially resulting in surface damage [6].

Nowadays, the most widely accepted explanation for the occurrence of surface erosion in presence of cavitation involves the violent implosion of vapor bubbles that occurs near solid walls. When a bubble is away from a solid wall, under free-flow conditions, the collapse is symmetrical and no erosion on the surface is detected. On the contrary, when the collapse occurs near a solid surface, it exhibits asymmetric characteristics, forming a rapidly accelerating liquid jet that enters the bubble from the side opposite to the wall, as visible in stages 1, 2 and 3 of Fig. 1 [7]. This collapse mechanism leads to two phenomena that can cause erosion damage, namely *"micro-jet"* and *"spherical micro-bubble collapse"*.

Experimental evidence shows, firstly, that the high-speed liquid jet impact on the wall can generate localized forces able to cause plastic deformation of the metal. This corresponds to stage 4 in Fig. 1. Secondly, following this impact, the flow moves radially and outwards, causing whirling structures, within which further bubble formation occurs (stage 5 in Fig. 1). This leads to the formation of several small bubbles (characterized by a diameter in the order of μm) arranged in a ring-like structure, which, due to their high surface tension forces, maintain a spherical shape during collapse. However, the rapid collapse of these micro-bubbles (stage 6 in Fig. 1) generates high-pressure shockwaves very close to the surface (stage 7 in Fig. 1), able to deform the material.

The collapse of a single bubble is extensively analysed in different studies by both CFD simulations and experiments. Among these studies, the most relevant one is that of Dular et al. [7], as they introduce an innovative methodology combining synchronized high-speed imaging of bubble collapse and surface deformation. This approach allows for the direct identification of the leading phenomenon in the erosion mechanism. Some results of this study are reported in Fig. 2(a) and (b) and suggest that the spherical micro-bubble collapse phenomenon is the most intense. For the example shown in Fig. 2(a), where the collapse occurs at a dimensionless wall distance of the bubble equal to 0.9, Fig. 2 (b) reveals that the damaged volume due to the spherical micro-bubble collapse is one order of magnitude greater than the one caused by the

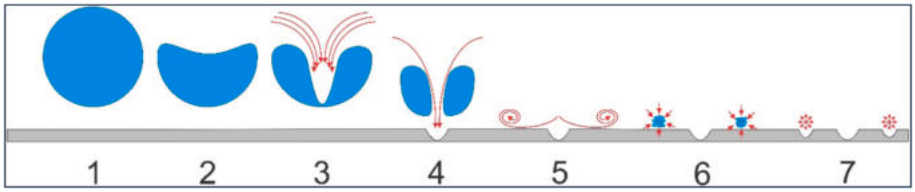

Fig. 1. Mechanisms of near-wall bubble collapse and erosion [7].

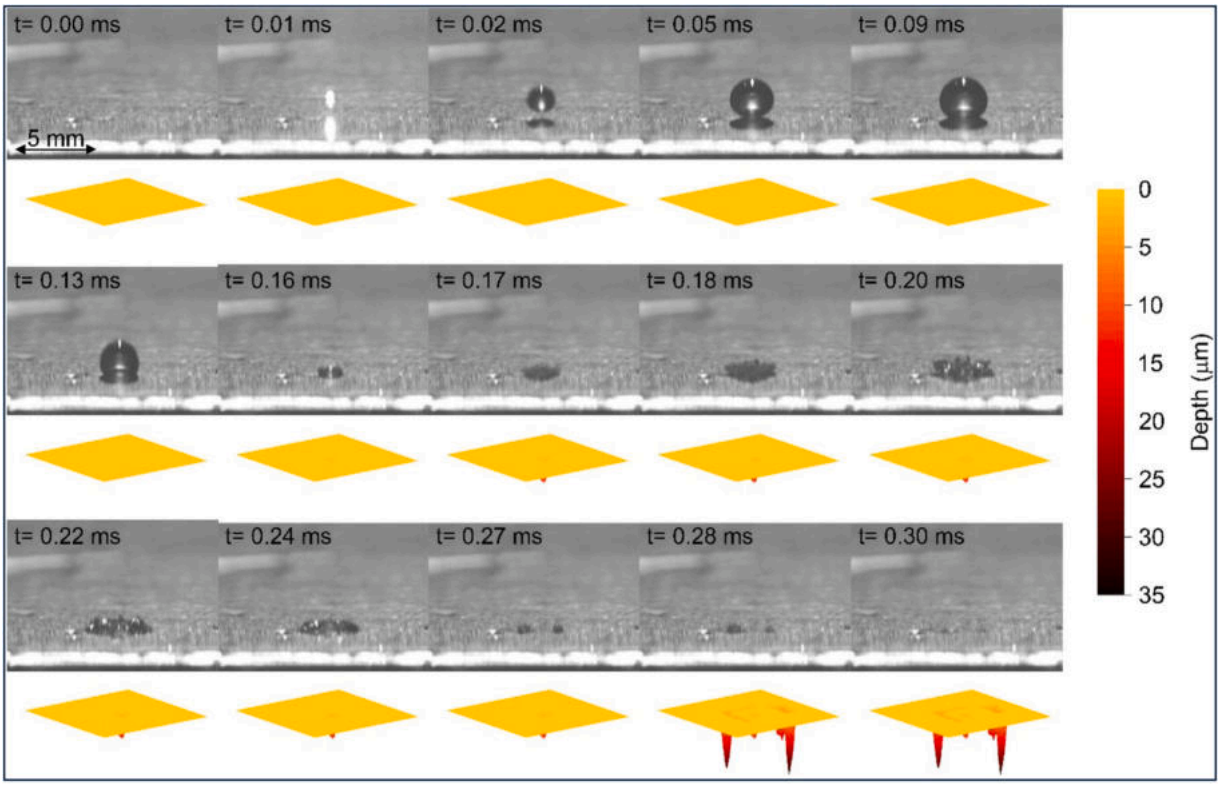

a)

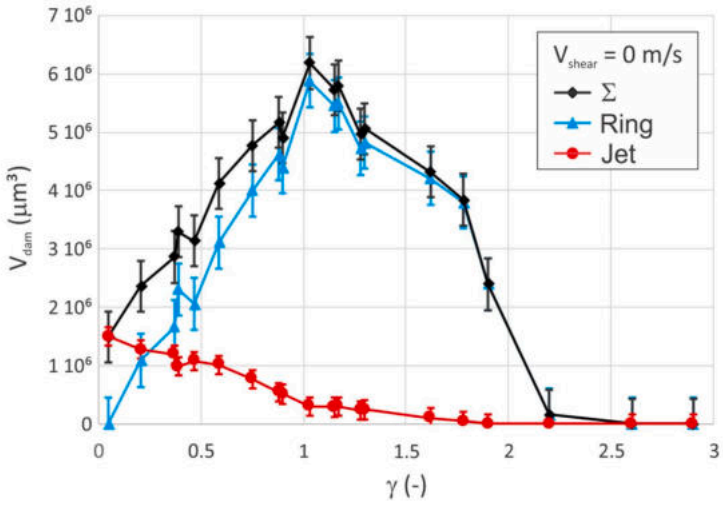

b)

Fig. 2. a) bubble and damage for collapse occurring at a dimensionless distance (γ) of the bubble from the wall of 0.9; b) damage as a function of γ [7].

micro-jet. Another interesting conclusion of [7] is that these results are valid as long as fluid motion is absent. In presence of shear flow (i.e. with relative velocity between liquid and wall), the surface deformation is exclusively caused by the micro-jet. In fact, the relative velocity prevents the formation of the whirling structures that generate the micro bubbles. In addition, the resulting damaged volume due to the micro-jet (for each tested dimensionless distance) is comparable between the two conditions. In other words, the red curve in Fig. 2(b) is similar with and without relative velocity between liquid and wall. Therefore, in case of fluid motion, a much lower erosion damage has to be expected.

Thanks to the advancements in Computational Fluid Dynamics (hereafter CFD), the industrial interest towards cavitation simulation and correlation with surface damage has grown significantly in the last years. As a consequence, several models have been developed for damage prediction. Based on the approach adopted for the cavitating flow simulation, these models can be classified into three main categories [8]. The first employs a Eulerian-Lagrangian approach, where the liquid phase is treated as a continuum in a Eulerian framework, while nuclei and micro-bubbles are modelled as a dispersed phase using a Lagrangian approach [9]. The second category adopts a Eulerian-Eulerian approach with a physics accounting for compressibility, aiming to fully capture bubble implosion dynamics and directly compute the intensity of the emitted pressure waves [10,11]. The third category relies on a homogeneous incompressible solver to simulate cavitating flow, establishing a relationship between vapor structures and erosion intensity through different parameters, based on characteristic

quantities of the cavitation phenomenon. Among these categories, only the third approach is actually feasible for engineering applications, due to the low computational cost. Instead of directly simulating the collapse, models belonging to the third-category can be directly implemented at the postprocessing stage. Some of these models are based on the energy cascade theory proposed by Patella [12], demonstrating good accuracy across various applications like diesel injectors [5], hydrofoils [13,14] and marine propellers [8]. Dular et al. [15] proposed an indirect erosion model based on jet velocity and yield strength of the considered material. Peters et al. [16] further developed this model by introducing a dimensionless erosion intensity coefficient.

In the context of boiling, numerical simulations have been extensively adopted in the last years to study bubble condensation. However, most of these studies focuses on the condensation of bubbles rising freely in a quiescent cold bulk or in a subcooled boiling flow, neglecting the influence of a solid wall and the related potential damage. Only in [17] the condensation process of a near-wall bubble is extracted from subcooled boiling, and it is investigated using a numerical method. In particular, the condensation mechanism is studied by varying different parameters such as liquid subcooling, bubble size and bubble-wall distance. The results indicate that, for dimensionless distance lower than 1.5 and liquid subcooling of at least 30 K, the condensation occurs in the form of asymmetric collapse of the bubble, which generates a micro-jet directed towards the wall, following a mechanism similar to the one observed in cavitation. The main difference lies in the fact that, for growth and condensation of a boiling-related bubble, the driving force is primarily the temperature difference between liquid and vapor, i.e. the level of liquid subcooling, instead of a pressure difference. However, jet velocities calculated in [17] are significantly lower than those observed in cavitation phenomena. As a demonstration, Fig. 3 reports the velocity fields proposed in [17], for different subcooled conditions, during bubble collapse. As visible, the highest calculated velocity is 3.8 m/s. In [7], the highest velocity measured for the micro-jet due to the cavitation-related bubble collapse shown in Fig. 3 is 92 m/s. In the first

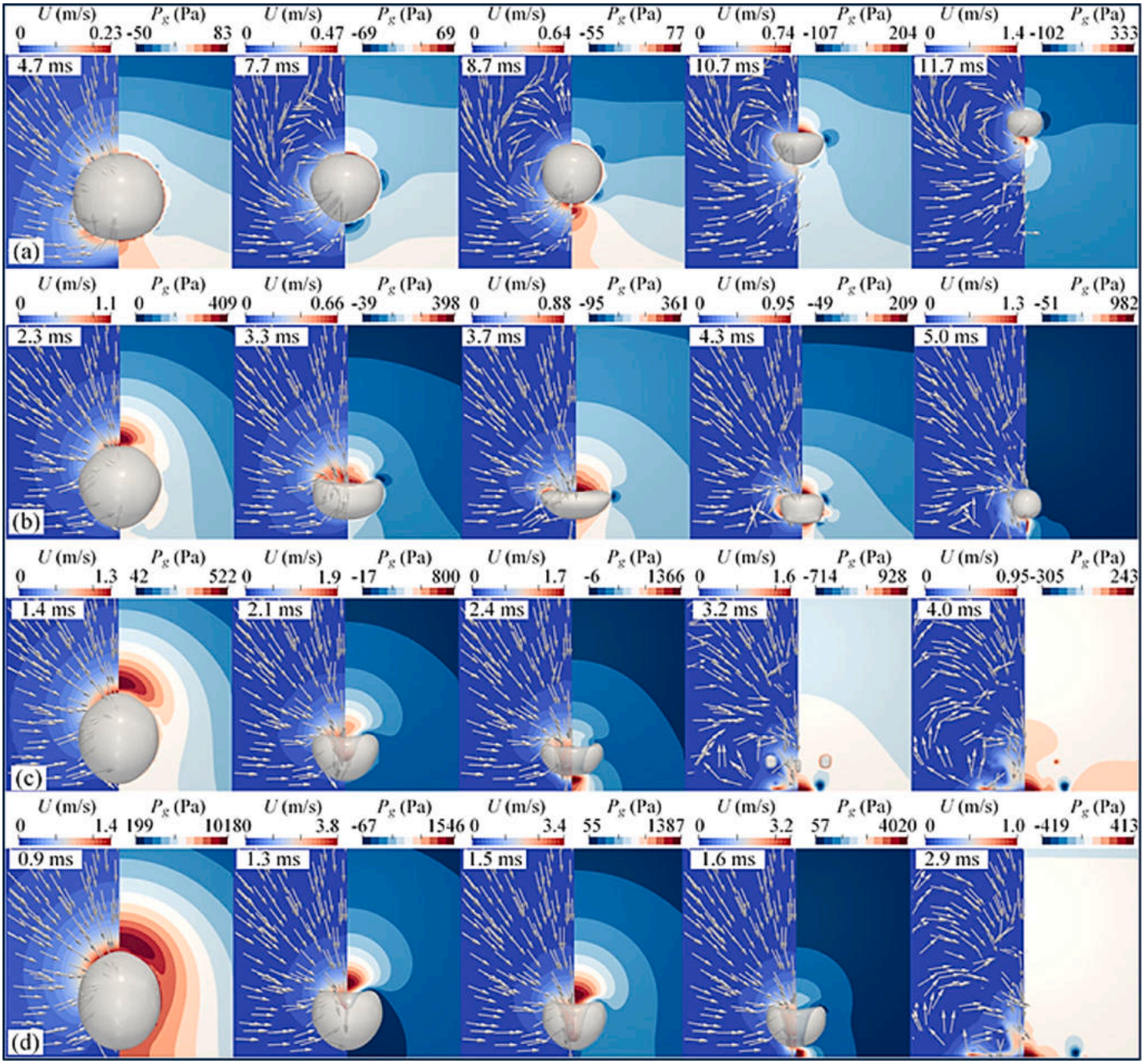

Fig. 3. Effect of liquid subcooling in terms of velocity field and pressure contour on bubble collapse; ΔT_{sub} = (a) 10, (b) 20, (c) 30 and (d) 40 K [17].

case, the velocity is roughly 24 times lower. Applications where higher jet velocities have been associated with boiling phenomena include heated wires [18,19] and laser heating of liquids through a fiber optic [20,21,22]. Also in these cases, bubble implosion is triggered by the high level of subcooling between vapor inside the bubble and surrounding liquid, but the resulting jet direction is opposite to the wall [22], because the different geometric boundary conditions significantly alter the dynamics of the phenomenon.

Therefore, in the light of the existing literature on erosion phenomena related to both boiling and cavitation, it is reasonable to state that the characteristic velocity of micro-jets due to the collapse of boiling-related bubbles is too low to cause significant erosion damage. In fact, in cavitation-related bubble collapse, the erosion due to micro-jet is already weak compared to the one due to spherical micro-bubble collapse. Then, in case of boiling, the characteristic velocity of micro-jets is more than one order of magnitude lower. As a result, the only phenomenon capable of causing surface deformation in presence of boiling is supposed to be the spherical micro-bubble collapse.

Since boiling has rarely been associated to erosion, no specific models were developed in the past to quantify the surface damage. Unfortunately, the consolidated erosion models available in literature have been developed for cavitation and cannot be applied in the context of boiling, as the characteristic quantities of the involved phenomena are different. For this reason, this paper proposes an erosion model which is synthetized by a novel parameter incorporating the characteristic quantities of the boiling phenomenon. The goal is the definition of a parameter able to estimate potential surface damage via a post-processing analysis of 3D-CFD results. The predictive capability of the parameter is assessed by comparing the areas of the cooling circuit, indicated by the parameter itself as high-risk regions, with the locations where severe damage is experimentally observed.

The paper is structured as follows. Firstly, the experimental setup is introduced, detailing the engine global parameters and the operating conditions of the cooling circuits. The positions within the investigated circuits where surface damage is experimentally observed are also presented. Then, the adopted CHT model is described, with a focus on the CFD methodology implemented to capture the multiphase physics of the problem. In order to identify the areas prone to erosion, the novel erosion parameter is outlined. Finally, the results of the CFD simulations are presented. The engine thermal field is validated against experimental data, at first. Then, the distribution of the erosion parameter is analysed and the predictive capabilities are discussed.

2. Experimental Apparatus

2.1. Engines and operating conditions

Two engine geometries characterized by similar cooling circuits are investigated in this paper. For the sake of confidentiality, they are referred to as engine A and B respectively. The investigated powertrains are current-production multi-cylinder direct-injection spark-ignition turbocharged units, whose main characteristics are reported in Table 1. The first engine is analysed only at one operating condition, characterized by full load (wide open throttle, WOT) and 7500 rpm of revving speed. The second one is investigated at two different operating conditions, namely 7500 rpm WOT and 2900 rpm part-load.

The conditions of the cooling circuits are summarized in Table 2 and vary depending on the engine operation.

Table 1
Main features of engine A and B.

B/S	>1
BMEP	>20 bar
Power	>700 CV

Table 2
Operating conditions of the cooling circuits.

Engines A and B at 7500 rpm WOT	
Mass Flow Rate	3.1 kg/s
Pressure Outlet	4.5 bar
Engine B at 2900 rpm part-load	
Mass Flow Rate	0.8 kg/s
Pressure Outlet	2.0 bar

2.2. Thermocouple measurements

During the experimental tests, a significant number of thermocouples is placed within the engine head, to measure the local temperature of the solid at the most critical positions. The goal is to verify that they do not reach excessive values able to affect the engine thermo-mechanical reliability. The thermocouples are distributed throughout the head. Specifically, those in the upper portion are positioned exclusively on the exhaust side, and they are adopted to monitor temperature of the solid between the exhaust ports and close to the exhaust flange. In the lower portion of the head, the sensors are useful to measure temperature close to the combustion chamber. In particular, the thermocouples are placed close to the spark-plugs, just above the cylinder dome. The data are available only for geometry B at 7500 rpm WOT. This operating point is the most interesting one for engine B, as it represents the peak power conditions, i.e. the most stressed one from a thermal point of view.

Thanks to the temperature measurements, a numerical-experimental comparison can be performed to validate the CHT model of the engine. In fact, the numerical temperatures can be obtained by probes positioned in the CHT model at the same positions as the experimental thermocouples, so that they can be compared with the test bench data. A preliminary validation of the CHT model in terms of solid temperatures is mandatory to verify the reliability of the model. Without a robust and validated model, it is not possible to focus the attention on detailed and complex phenomena such as boiling and erosion.

2.3. Erosion regions

Experimental observations by photos of sectioned engine and X-ray images as the ones shown in Fig. 4 reveal the presence of surface damage in specific areas of the investigated engine heads. The position of these damaged regions depends on both operating conditions and geometry of the cooling circuit. Such regions are presented in the following and are visible in Fig. 4.

- **Region 1**: relevant erosion phenomenon occurring in engine A, at 7500 rpm WOT. The erosion involves the region of the cooling circuit nearby the exhaust flange. In particular, in figure, a crack starting from the superficial erosion region is visible.
- **Region 2**: erosion phenomenon observed in an extreme portion of the circuit (i.e. in correspondence of the last cylinder of the bank), which is close to an exhaust port and it is characterized by almost stagnating flow conditions. This erosion phenomenon is less intense compared to that of Region 1 and it appears in engine B, at 7500 rpm WOT.
- **Region 3**: erosion phenomenon affecting the cooling circuit around the spark plug in engine B, at 2900 rpm part-load. In this case, the detected damage is the least intense among the three observed.

Thanks to the experimental images showing the erosion regions, it is possible to carry out a second numerical-experimental comparison to evaluate the capability of the novel erosion model to predict erosion areas and relative potential damage.

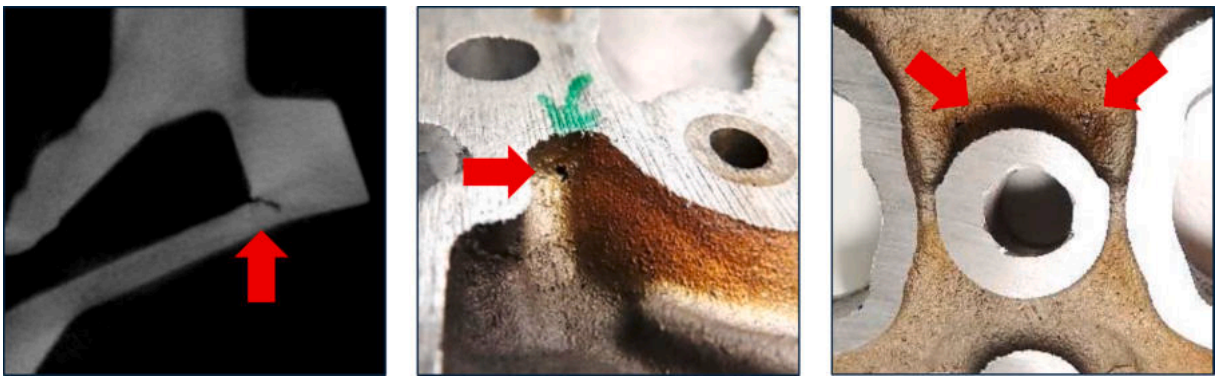

Fig. 4. From left to right, the erosion regions 1, 2 and 3 are visible. The first picture on the left is an x-ray image while the other two are photos.

3. CFD tool

The CFD tool employed in this work to analyse the boiling-induced erosion phenomena detected in the investigated cooling circuits is presented in the following. In particular, the tool consists in both a detailed CHT model of the engine and an erosion model synthetized in a parameter. The CHT model is created within STAR-CCM+ software licensed by SIEMENS DISW and it is described at first, with focus on computational domain, boundary conditions, physical and numerical setups and wall boiling model. Then, the erosion model is described in detail. The CFD tool as outlined below is adopted for both the investigated engines.

3.1. Computational domain

For an accurate virtual representation of the engine, it is essential to have a detailed CHT model including all the components, capable of predicting the heat fluxes among them and, thus, the thermal field. First of all, the adopted CHT model is characterized by the simultaneous presence of both solid and fluid domains. The latter is represented by the cooling circuit, while the former includes all the solid components such as head, block, gasket, liners and valves.

The presence of several components within the computational domain results in a significant computational cost for each simulation. Therefore, it is necessary to optimize the mesh to minimize the number of cells as much as possible. Given the different complexity of the physics, fluid and solid regions are treated separately, with different discretization criteria for each one.

The fluid region is discretized by a polyhedral mesh in the bulk and two prismatic layers near the walls. Dedicated refinements are reserved to specific regions of the cooling circuit. In the block, the cell size is reduced close to the liners, while, in the head, refinements are adopted for the narrow straight channels, as visible in Fig. 5. Refining the discretization in these regions is crucial, because they are characterized by high heat transfer and, hence, presence of boiling. As for the near-wall flow modelling, the height of the prismatic layers is properly chosen, in respect of the grid quality, to keep y^+ values as high as possible. In other words, a High-Re grid is adopted. The reason is that it is the only one compatible with the nucleate boiling model. In fact, vapour formation occurs in the near-wall cells. If these are too small (as it occurs in a Low-Re approach), the vapour concentration in the first layer quickly reaches values close to unity. This (numerical) phenomenon is equivalent to what is physically observed in the film boiling regime and, consequently, it leads to an increase in the temperature of the wall-adjacent cells due to the lower vapour thermal conductivity. This temperature rise activates the correction for the boiling heat flux proposed in Eq. (1) and implemented in the adopted code.

$$max\left[0, min\left(\left(\frac{T_{wall} - T_{cell}}{T_{wall} - T_{sat}}\right), 1\right)\right] \tag{1}$$

The goal of this correction is to extend the boiling model beyond its original range of applicability (namely nucleate boiling), in order to capture the reduction in heat flux that occurs when the film boiling regime is reached. However, the analysis of the wall superheat temperature in the present case shows values that are fully consistent with nucleate boiling conditions (i.e. below 30 K), indicating that the correction is not actually required. As a result, when a Low-Re grid is adopted, the software erroneously applies a boiling heat flux reduction even if film boiling is not present.

Similarly, the solid regions are refined only in areas where high thermal gradients are expected, i.e. close to the combustion chamber and exhaust port walls. However, since the modelling of the solid regions is less complex, larger polyhedral cells are used compared to those in the fluid domain and the prismatic layers are not used. The result is a global spatial discretization that is both accurate and computationally efficient.

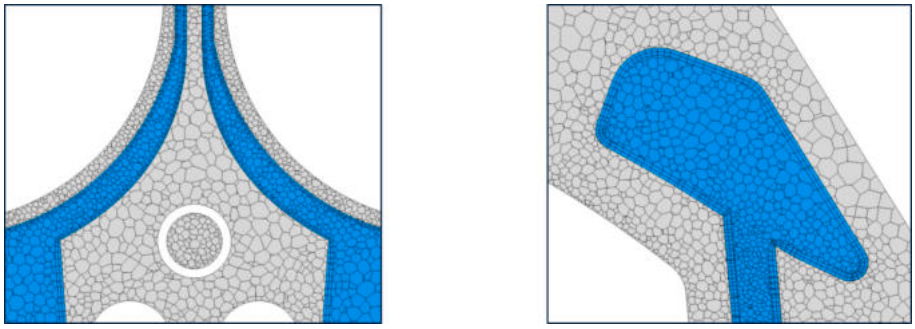

Fig. 5. Sections of the computational grid; on the left, a section near the liner; on the right, a section of the head.

3.2. Boundary conditions

For the fluid region (cooling circuit), mass flow rate and temperature of the coolant at both inlet and outlet are set to replicate the actual test-bench operating conditions. The effect of the lubricating circuit (not simulated) is mimicked by a pair of properly defined heat transfer coefficient and reference temperature. The same approach is adopted to consider the heat transfer with the environment.

As for the solid region, since the accuracy of the simulations in terms of temperature and wall boiling estimation within the engine heavily depends on the choice of proper thermal boundary conditions (BCs), particular care is paid to the distribution of the heat fluxes on the components facing the combustion chamber. In this regard, the gas-to-wall heat fluxes are derived from 3D-CFD in-cylinder simulations. Since pistons are not included in the computational domain (because they cannot be placed in a preferential fixed position [23]), an ad hoc heat flux distribution is applied on each liner, able to simultaneously account for heat transfer from piston, convection from hot gases of combustion (provided by in-cylinder simulations), and frictions due to piston motion inside the cylinder [24,25].

Finally, a heat source is applied at the exhaust flange to account for the heat transfer from the exhaust manifold to the engine head.

3.3. Physical and numerical setups

The coolant is a 50/50 mixture of water and ethylene glycol, whose physical properties at the operating temperatures and pressures are provided by the supplier. As for the metal components, each one is characterized by specific properties (such as density and thermal conductivity) based on the material, which are similarly provided by the engine manufacturer.

A steady-state approach is adopted for both solid and liquid domains. For completeness, it is interesting to point out that also an unsteady approach is investigated, with the same results (not reported in the following for brevity). As for the cooling circuit, RANS equations are adopted, with spatial discretization carried out using second-order-accuracy numerical schemes. For the turbulence modelling, the Realizable k-ε is selected, which was satisfactorily adopted by the authors in previous works involving multi-phase flows [25,26]. For the near-wall flow modelling, the "Two-Layer All-y^+ Wall Treatment" is employed. This choice is necessary due to the presence of both small flow passages and low velocities in certain regions of the cooling circuit, that makes it impossible to satisfy the requirements of a high Reynolds wall treatment, i.e. $y^+ > 30$, throughout the domain. Further details on the near-wall treatment and on the calculation of the wall quantities (namely wall shear stress and convective wall heat flux) can be found in [27].

To accurately represent the boiling phenomenon, a multiphase modelling approach is required. In this study, the Volume of Fluid (VOF) multiphase model within the Eulerian framework is employed to simulate both liquid and vapor phases. This is a one-fluid approach, meaning that a single set of governing equations is solved for an equivalent mixture-fluid, whose physical properties are calculated as functions of physical properties and volume fractions of the constituent phases. The spatial phase concentrations within the domain are defined by an additional phase fraction transport equation.

The effects of interaction between liquid and vapor phases, such as drag, heat transfer and phase change are captured via terms defined by additional sub-models. Further details can be found in [27].

3.4. Wall boiling model

In case of nucleate boiling at the walls (the only boiling regime accounted for in this work), the primary goal is to model phase change phenomena from liquid to vapor, estimating both the vapor production rate and the additional wall heat flux. Indeed, the main effect associated with wall boiling is the increase of total heat flux removed from the surface, as expressed by Eq. (2). Compared to the convective contribution, the increment is due to both enhancement of motion within the liquid and heat absorbed during bubble formation.

$$q_{TOT} = q_{conv} + q_{bw} \tag{2}$$

The adopted nucleate boiling model is based on the formulation proposed by Rohsenow [28]. According to this model, originally developed for pool-boiling regimes and subsequently extended to flow-boiling conditions, boiling occurs at the liquid/solid interface when the wall surface temperature T_{wall} exceeds the saturation temperature T_{sat}. The additional wall heat flux due to boiling is modelled using an empirical correlation expressed by Eq. (3), which depends on the wall superheat.

$$q_{bw} = \mu_l h_{lat} \sqrt{\frac{g(\rho_l - \rho_v)}{\sigma}} \left(\frac{c_{p_l}(T_{wall} - T_{sat})}{C_{qw} h_{lat} Pr_l^{n_p}} \right)^{3.03} \tag{3}$$

μ_l, ρ_l, c_{p_l} and Pr_l are dynamic viscosity, density, specific heat, and Prandtl number of the liquid phase. g is the gravitational acceleration, ρ_v is the vapor-phase density and σ is the surface tension at the liquid–vapor interface. C_{qw} and n_p are empirical constants. A value of n_p equal to 1 is commonly accepted in the literature for the type of coolant used in this work [29,30,31]. Conversely, the parameter C_{qw} exhibits greater variability in the available papers, and it is often employed to calibrate the boiling heat flux [30]. Therefore, in this study, C_{qw} is set to 0.004 which well agrees with the existing literature [32,33,34] and also leads to a satisfying match with the experimental data.

The production of vapor at the wall-adjacent cells is computed based on the wall heat flux, as indicated by Eq. (4).

$$\dot{m}_{ew} = \frac{C_{ew} q_{bw}}{h_{lat}} \tag{4}$$

C_{ew} is an additional model constant stating how much of the boiling heat flux is used to form vapor bubbles. C_{ew} is set to 0.1, namely the default value, as it is the result of extensive validation by SIEMENS DISW [35].

3.5. Erosion parameter

In absence of erosion model specifically designed for boiling, as confirmed by the literature review, this paper proposes a dedicated approach inspired by erosion models commonly adopted in cavitation studies. From a physical standpoint, as anticipated in the introduction, erosion cannot be related to micro-jet in presence of boiling, because of the low jet velocities. Therefore, the spherical micro-bubble collapse can be reasonably assumed as the leading erosion phenomenon. In other words, the present work aims at proposing an erosion model in case of boiling, which justifies the damage with the collapse of micro-bubbles generating high-pressure shockwaves able to deform the material. Once the physics is clarified, it is necessary to point out that the proposed model does not provide for direct simulation of the implosion dynamics. It estimates potential surface damage through a post-processing analysis, defining an erosion parameter that incorporates characteristic quantities of the boiling phenomenon. These quantities are presented in the following along with the final expression of the erosion parameter.

The results presented in [17] indicate that the condensation of a vapor bubble follows a mechanism similar to cavitation, when it is sufficiently close to a solid wall and high liquid subcooling is present, and the collapse velocity increases with the subcooling level defined by $\Delta T_{sub} = T_{vapor} - T_{liquid}$. Therefore, the proposed parameter should exhibit a direct dependence on this quantity. The higher ΔT_{sub} is, the greater the erosion parameter (and, thus, the risk of damage) should be. From a modelling perspective, assuming that the vapor temperature remains constant at the saturation value and the liquid temperature can be approximated by the cell temperature (actually corresponding to the mixture temperature), ΔT_{sub} is computed as the difference $T_{sat} - T_{cell}$.

Such assumptions are validated through a simulation based on the Eulerian Multiphase (EMP) approach, which is the only two-fluid method within the Eulerian framework that allows an exact computation of this temperature difference. In fact, both T_{vapor} and T_{liquid} are available, thanks to separate energy transport equations for the different phases. The EMP simulation is discussed in detail in the Appendix.

A second quantity for the definition of the erosion parameter deals with the presence of the spherical micro-bubble collapse. Since the presence of this erosion phenomenon is experimentally observed exclusively in absence of relative velocity between flow and wall [7], it is reasonable for the erosion parameter to account for fluid velocity. In other words, stagnation regions are identified as those where erosion is more likely to occur. Consequently, the erosion parameter should be inversely proportional to the fluid velocity. In order to avoid mesh dependency, instead of using the actual fluid velocity computed at the near-wall cell centroid, the friction velocity u_τ is employed. According to the adopted High-Re approach, u_τ is calculated as in Eq. (5), where k is the turbulent kinetic energy at the near-wall cell centroid and C_μ is a turbulence model constant equal to 0.09.

$$u_\tau = \sqrt[4]{C_\mu k^2} \tag{5}$$

A third key quantity for the definition of the erosion model is related to the temperature field. In order to understand this selection, it is necessary to consider three aspects. Firstly, strong bubble nucleation occurs at the walls where the average liquid temperature (assumed equal to the cell temperature) is close to saturation due to the high temperature reached by the metal. Secondly, as suggested in [17], low liquid temperature is necessary to ensure strong subcooling conditions, thus violent bubble implosion and potential damage. Thirdly, the lifetime of vapor bubbles is extremely short, in the order of milliseconds when subcooled conditions are met [7,17]. Consequently, it is reasonable to assume that once formed, a bubble travels only for a short distance, especially if it is in a stagnation region. Combining the three aspects, bubble formation has to necessarily take place in areas with steep thermal gradients in the surrounding liquid. In this way, according to the extremely short lifetime of the bubbles, massive formation occurs and, after short displacement, a much colder region enabling impulsive condensation mechanism can be encountered. In the light of this, the erosion parameter must also be directly proportional to the temperature gradient. In particular, only the tangential component of the thermal gradient (i.e. the one along the wall) is considered, as it is the one actually experienced by the bubbles moving close to the surface. In this regard, a schematic representation of the thermal gradient is reported in Fig. 6. It is useful to point out that the interest is focused on the liquid thermal gradient. As already commented, the cell temperature is assumed as liquid temperature, thus the temperature gradient included in the erosion parameter is the gradient of the thermal field calculated by the transport equations. For completeness, it is useful to point out that the magnitude of the tangential component is adopted. In fact, the interest is in the presence of a strong gradient, regardless the specific direction.

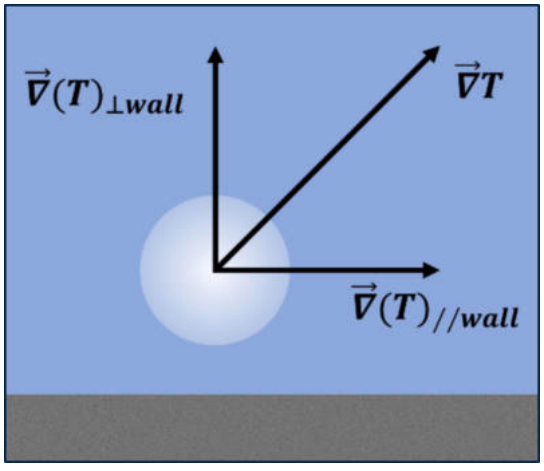

Fig. 6. Decomposition of the temperature gradient that a vapour bubble faces close to a wall.

In addition to the aspects considered so far, it is crucial for the erosion parameter to also account for the presence of vapor in the fluid, represented by α_v (i.e. vapor volume fraction) within each cell. Including this characteristic quantity of the boiling phenomenon not only helps to distinguish the regions where vapor is actually present (so where collapse can occur), but it also emphasizes the importance of the regions with higher vapor concentration. In fact, this means higher bubble number and/or bubbles with larger diameters, which translate in larger number of collapses and/or stronger collapsing phenomena. Therefore, the erosion parameter has to be somehow proportional to α_v.

In conclusion, considering all the aspects discussed above, the erosion parameter reported in Eq. (6) is defined. The GEP, namely GruMo (Gruppo Motori research group) Erosion Parameter, highlights the regions of the solid surface where the conditions of potential damage are met.

$$GEP = \frac{\alpha_v \cdot \Delta T_{sub} \cdot \left|\vec{\nabla}(T)_{//wall}\right|}{u_\tau \cdot T_{sat}^2} \tag{6}$$

As visible in Equation (6), T_{sat}^2 is added to the definition. This term does not alter the parameter distribution, since the saturation temperature remains roughly constant in the boiling regions. It is introduced only to scale down the values of the parameter itself. Due to the high thermal gradient values, without T_{sat}^2, the parameter would assume excessively large values, which are impractical to use.

Thanks to this modelling approach, GEP can be easily implemented to be used in both research and industry. In fact, once the necessary quantities are computed by a CFD simulation, the parameter can be easily defined through a scalar function and plotted on the walls. In this regard, it is useful to specify that all the quantities involved in the calculation of GEP are provided by the CFD code at near-wall cell centroids (i.e. centroids of the cells in contact with the walls) but the parameter is plotted at the walls. Specifically, it is visualized on the near-wall cell faces corresponding to the walls. This is due to the fact that, at least in STAR-CCM+, actually only the temperature gradient is available at the cell centroid. The component parallel to the wall is obtained via post-processing by projecting the gradient vector onto the cell face laying on the wall. Therefore, $\vec{\nabla}(T)_{//wall}$ is available only at the cell face, although the original quantity ($\vec{\nabla}(T)$) is provided by the code at the centroid.

Before moving to the results, it is necessary to note that the proposed parameter accounts for neither the mechanical properties of the solid surface material nor the operating time. As obvious, erosion depends also on them. Rather, GEP focuses on the fluid domain, by pointing out the presence of conditions that can potentially lead to erosion. Then, prediction of damage occurrence and quantification would also necessitate mechanical properties and time, which are not considered at this stage of model development. In addition, apart from T_{sat}^2, a direct proportionality is considered between GEP and the different terms. However, nothing prevents that a different proportionality (super- or sub-linear) is considered in the future, to increase or diminish the impact of the different contributions.

Moreover, considering the erosion mechanism, it is implicit in the conceptualization of the parameter that GEP is mainly intended to be adopted with bubbly flow regime. In fact, although the presence of small bubbles can be detected also in more complex regimes such plug and slug ones, they mainly characterize the bubbly flow regime and their presence is mandatory for the erosion mechanism previously described,

which starts with bubble collapse.

4. Results

This section presents the results of the CFD simulations adopted to analyse the boiling-induced erosion observed in the investigated engines. The predictive accuracy of the CFD models is evaluated with two different sets of comparisons. The first is in terms of pointwise temperature measurements, while the second examines the distribution of the erosion parameter in areas where surface damage is experimentally detected.

4.1. CHT model validation

A validation of the CHT model in terms of pointwise temperature distribution is necessary to verify the capability to properly capture the main phenomena affecting the thermal field of the engine, such as heat transfer (conduction and convection) and boiling. For this purpose, the experimental data from the thermocouples installed within the engine at the test bench are used to validate the CHT modelling framework presented in the previous section. Fig. 7 presents the comparison between the values provided by the numerical probes positioned in the CHT model and the experimental counterparts. It is useful to remember that this comparison is limited to engine B at 7500 rpm WOT, as it is the only case for which experimental temperatures are available. Fig. 7 already shows the difference between CFD and experimental values and, as visible, a good correlation between the CHT model and the actual engine is obtained. In fact, the error between predicted and measured temperatures is always lower than 25 K for almost all the measurement locations, i.e. always lower than 6 %.

4.2. Erosion parameter validation

First of all, the distribution of the erosion parameter in the cooling circuit is examined in Fig. 8, for the analysed engines and conditions. For a better comparison, also the experimental images are reported in figure. Peaks of the parameter can be noticed exactly at the areas where there is experimental evidence of surface damage. In other words, Fig. 8 shows a one-to-one correspondence between the portions of the cooling circuits where GEP is maximum and the experimentally detected erosion regions. Therefore, the analysis of the erosion parameter reveals strong correlation between CFD simulations and experiments. It is important to point out that, despite the definition of the parameter, GEP values may not be null elsewhere in the circuit, where there is no visible damage. However, focusing on the peak values, they match with the erosion regions.

As previously discussed, the erosion parameter proposed in this study indicates a connection between potential boiling-related erosion damage and local thermo-fluid dynamic properties of the flow. Therefore, it is interesting to analyse the values assumed by the characteristic quantities composing the parameter, in the coolant domain in proximity of the eroded areas. In this way, the correlation between key characteristic quantities and erosion can be highlighted.

The erosion parameter proposed in this paper is mainly based on the combined effect of volume fraction of vapor, liquid subcooling, tangential component of the temperature gradient and flow velocity, which are shown in the following in correspondence of the erosion regions.

As visible in Fig. 9(a), the results indicate strong correlation between vapor distribution predicted by the multi-phase model and areas where the experiments show surface damage. In particular, high vapor concentrations are found in the erosion regions.

Subcooling condition and temperature gradient can be appreciated in Fig. 10, which reports the distribution of the subcooling level, namely $\Delta T_{sub} = T_{vapor} - T_{liquid}$, calculated at the fluid cells in contact with the wall (i.e. near-wall cells).

Firstly, as visible in Fig. 10, the erosion regions exhibit ΔT_{sub} values up to 50 K, that is the surrounding liquid temperature is significantly lower than that of vapor. As clarified in the previous paragraphs, this subcooled condition promotes the bubble collapse.

Secondly, by comparing Fig. 9(a) and 10, it is interesting to notice that the regions with the lowest values of ΔT_{sub} are also those with the highest vapor concentrations. In fact, as previously commented, if the liquid temperature (i.e. cell temperature) is already close to the saturation one, boiling is intense at the wall. However, as visible in Fig. 10, a minimal distance (in the order of mm) separates regions with low and high ΔT_{sub} values. In other words, when bubbles form in regions characterized by high liquid temperature, they can shortly move to "colder" portions of the circuit. Therefore, strong variations of liquid subcooling conditions can be noticed. Since the saturation temperature remains roughly constant, this implies high liquid temperature gradients. This confirms the strong correlation between erosion region and temperature gradient. Concluding, damage is experimentally noticed in regions where CFD simultaneously predicts high values of ΔT_{sub} and temperature gradient.

As a demonstration of the short life-time of the bubbles, a section reporting the volume fraction of vapour in correspondence of the erosion region 2 is shown in Fig. 9(b). Following the flow thanks to the velocity vectors, it can be noted that the vapour concentration quickly drops to negligible values. From another perspective, it is possible to say that only bubbly flow regime is established and it occurs locally because of the short life-time of the bubbles as a consequence of the strong

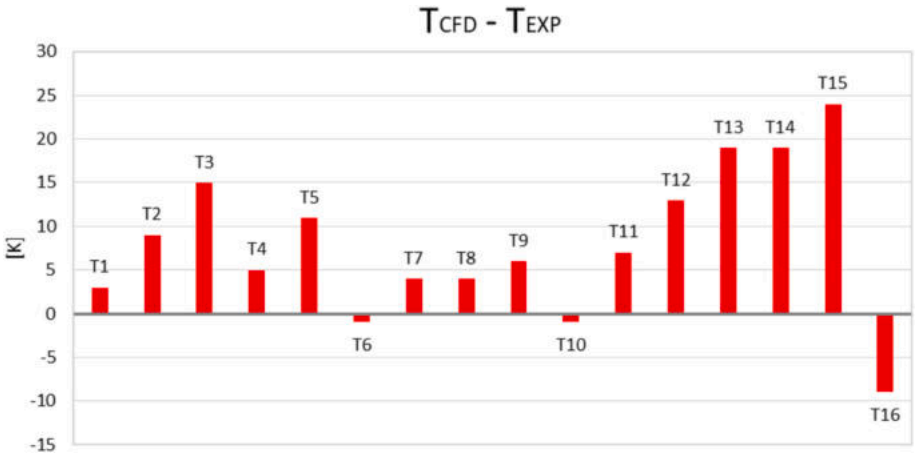

Fig. 7. Difference between numerical temperatures and experimental ones.

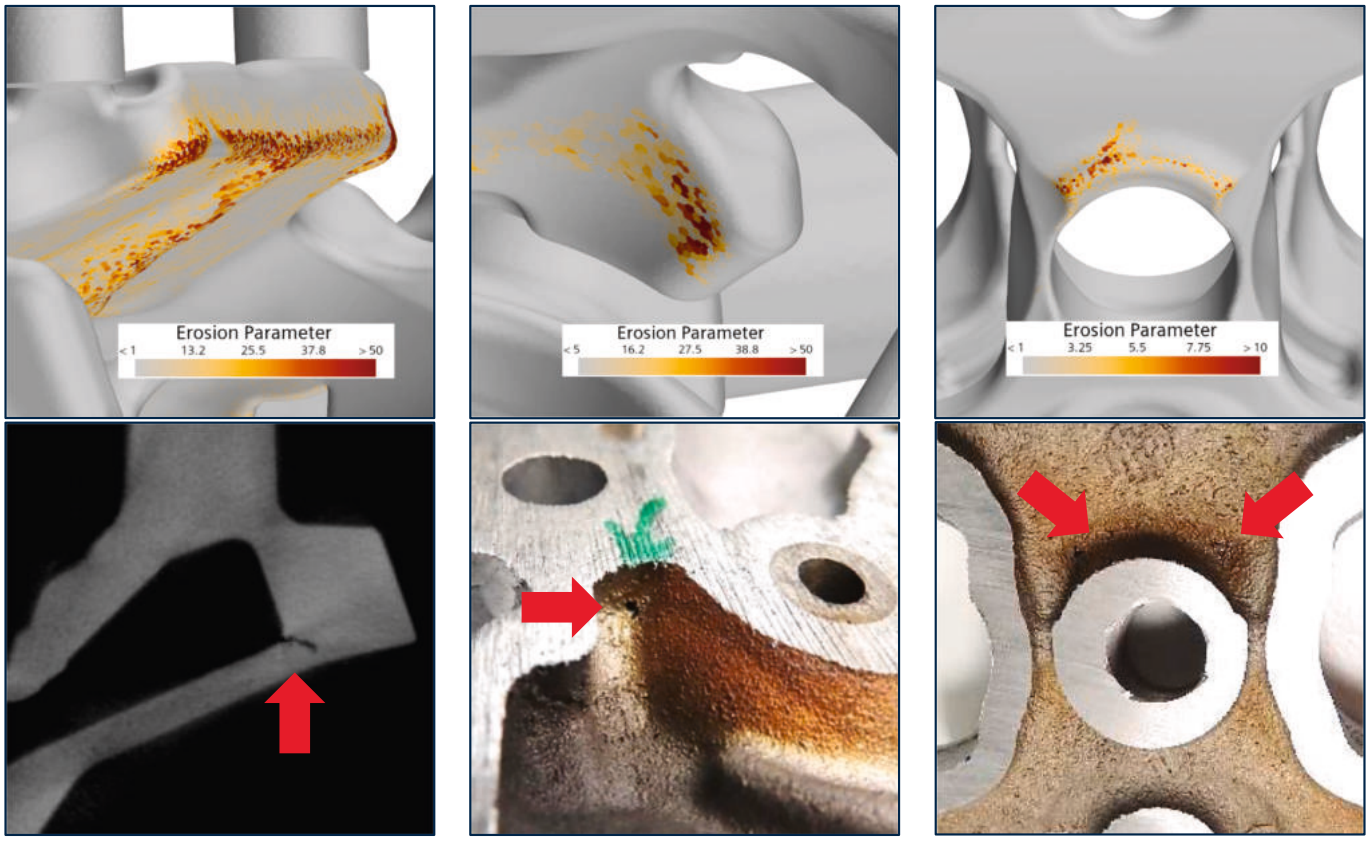

Fig. 8. In the top row, GEP field on the near-wall cell faces of the cooling circuits in correspondence of the regions characterized by erosion; in the bottom row, the experimental images of the erosion regions of the solids facing the cooling circuits.

subcooled conditions that are quickly met. In fact, the wall superheat is limited to small portions of the cooling circuits (mostly corresponding to the erosion ones), and there is no vapor mass formation and space enough to switch to more complex flow regimes.

Regarding the last characteristic quantity of the erosion parameter, i.e. the fluid velocity, it is essential to verify that the regions of interest coincide with flow stagnation zones. In Fig. 11, the distribution of the velocity magnitude computed at the centroids of the near-wall cells is shown. The analysis of the velocity field highlights that the cooling circuit geometry promotes the formation of flow stagnation zones exactly in the areas where surface damage is observed.

Considering all the investigated quantities, the presented findings support the hypothesis of the proposed erosion model that the primary phenomenon is the spherical micro-bubble collapse. In fact, damage regions are simultaneously characterized by presence of vapor, strong subcooled conditions, high temperature gradients of the liquid and almost stagnation of the flow. These thermo-fluid dynamic conditions form the perfect mix for the spherical micro-bubble collapse to occur. Therefore, not only GEP represents an effective parameter to predict potential damage, but it also implicitly confirms that the supposed leading phenomenon in the erosion mechanism is correct. Not by chance, GEP is conceived to be higher where the flow velocity is lower, according to the main hypothesis for the occurrence of the spherical micro-bubble collapse phenomenon.

Before moving to the conclusions, it is important to clarify a crucial aspect of GEP. Qualitatively, it is possible to state that the higher the erosion parameter value is, the faster the erosion process becomes. Quantitatively, it is very difficult to define a threshold value for GEP beyond which damage can be confirmed. The reason is related to both time and material properties.

Focusing on time, as shown by the different scales in Fig. 8, in the simulation at 2900 rpm the absolute values of the parameter are lower than those observed in the other two cases. Therefore, the identification of a threshold value above which damage can be expected has to be based on this specific simulation. Following this approach, a threshold value roughly equal to 5 can be identified. However, even lower GEP values may lead to damage. Simply, more time would be required for the erosion to occur. The point is that the search for a single threshold value is challenging as erosion is time-dependent. It is not an instantaneous process, but a gradual one that develops over time. Surface damage is not caused by the collapse of a single bubble, but the repeated collapse of numerous vapor bubbles, which progressively remove material from the surface. In this regard, it is possible to notice that the identified threshold applied to the other two cases at 7500 rpm WOT predicts potential damage also in regions where no experimental evidence of erosion is observed. The reason is that the experiments identify the regions showing peak values of the parameter, as they are the first to develop erosion and cause engine failure. With more time available for the operation (that is without failure), many other regions of the cooling circuit would probably manifest erosion in the experiments. Similarly, at 2900 rpm, more operating time may lead to erosion in regions characterized by GEP values lower than 5 and a new threshold should be identified. This interpretation is supported by the experimental data. In engine B, surface damage is observed in regions 2 and 3. However, the erosion in region 3 progresses at a slower rate as the damage is less evident on equal operating time. Examining the distribution of the erosion parameter in Fig. 8, it is evident that the maximum values in zone 2 are higher than those in zone 3, suggesting a direct correlation between erosion speed and parameter magnitude.

The second reason is related to the material properties of the surface involved in potential erosion. Interestingly, apart from the previously analysed regions pertaining to the cylinder head, a global assessment of the erosion parameter distribution reveals high values in some portions of the circuit in contact with the liner, especially at 7500 rpm WOT, for

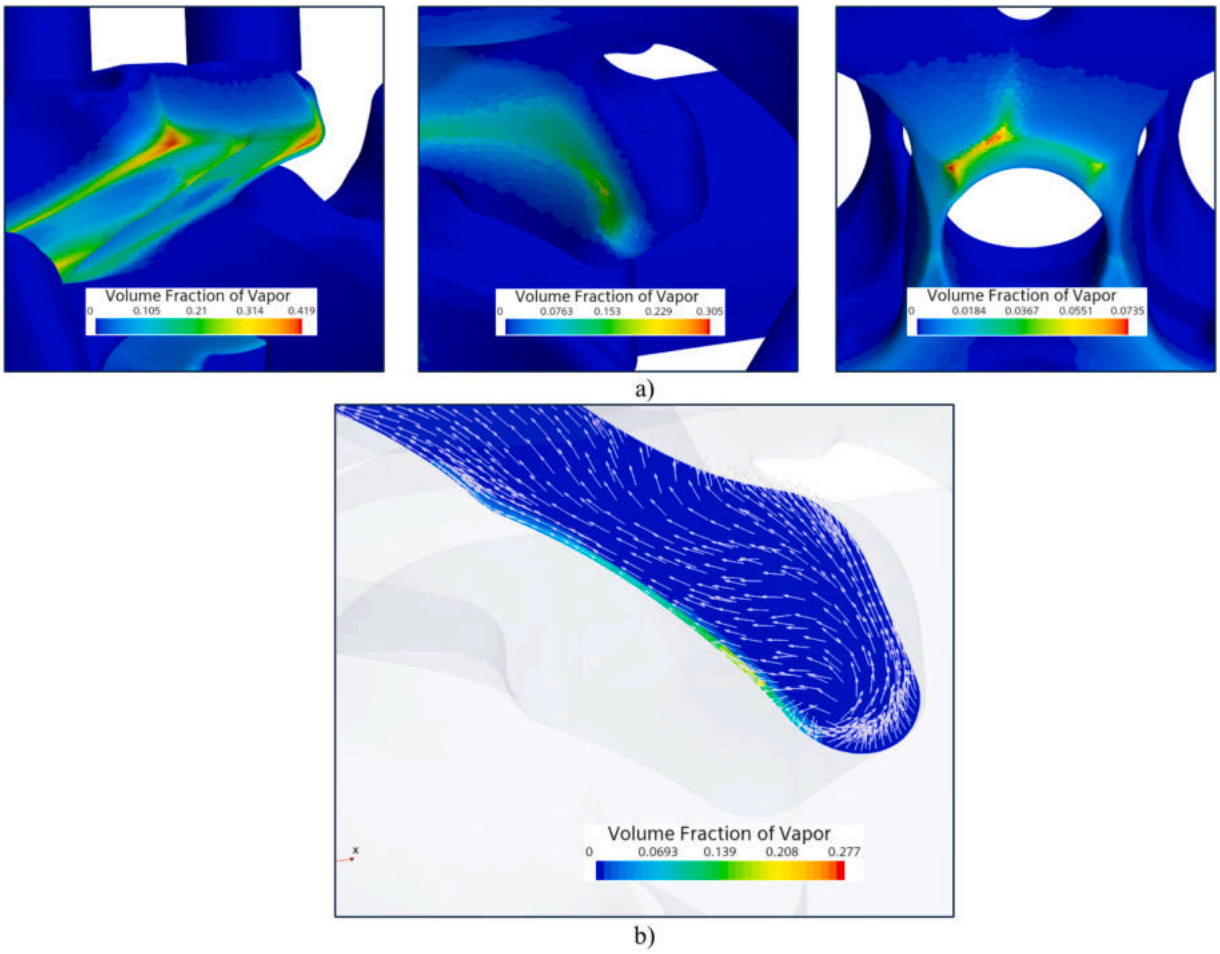

Fig. 9. a) vapor distribution in the near-wall cells of the cooling circuits, in correspondence of the regions characterized by erosion; b) section of the cooling circuit reporting volume fraction of vapour and velocity vectors, in correspondence of erosion region 2.

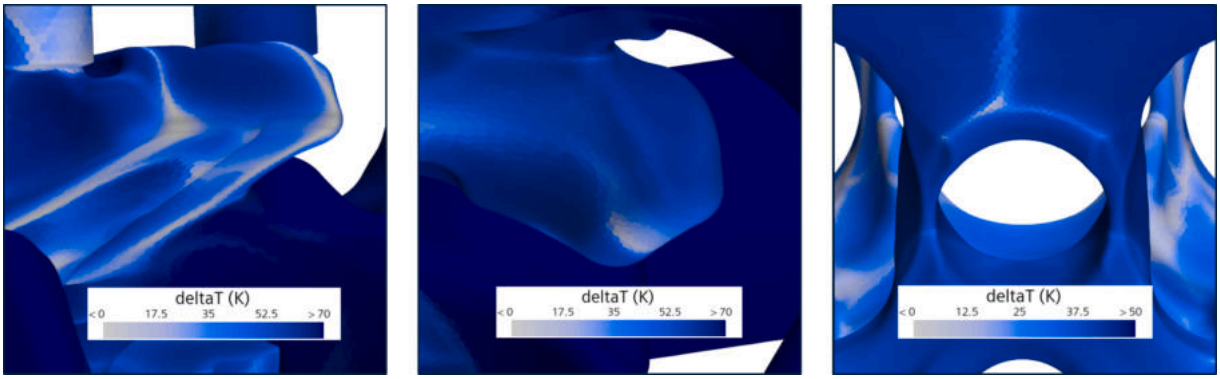

Fig. 10. Liquid subcooling level (ΔT_{sub}) in the near-wall cells of the cooling circuits, in correspondence of the regions characterized by erosion.

both the engines. Also in these regions of the block, the conditions for potential boiling-induced erosion are present. However, such conditions do not pose a significant structural concern, thanks to the mechanical properties of the involved materials. Engine head and liner are made of aluminium alloy and steel, respectively, i.e. materials with significantly different mechanical properties. As a result, despite the high GEP values in the circuit close to the liner, the superior tensile strength of steel substantially reduces the risk of damage. This represents the major limitation of the proposed erosion model. It only relies on characteristic quantities of the fluid domain, computed at the centroids of the fluid cells, preventing it, at least so far, from accounting for the mechanical properties of the solid. Therefore, the model can only predict conditions of potential damage and not the damage itself. This limitation is common to most cavitation erosion models and it points out the importance of a critical assessment. Based on the specific application, a critical evaluation of the fluid–solid interaction is essential to properly interpret the information provided by the parameter proposed in this work.

As for the identified GEP threshold and, more in general, concerning the GEP fields, it is necessary to point out that the proposed values depend on the adopted numerical setup. The modification of model constants such as C_{qw} can alter the presented outcomes (fields of vapour volume fraction, GEP, etc.) and lead to the definition of a new GEP

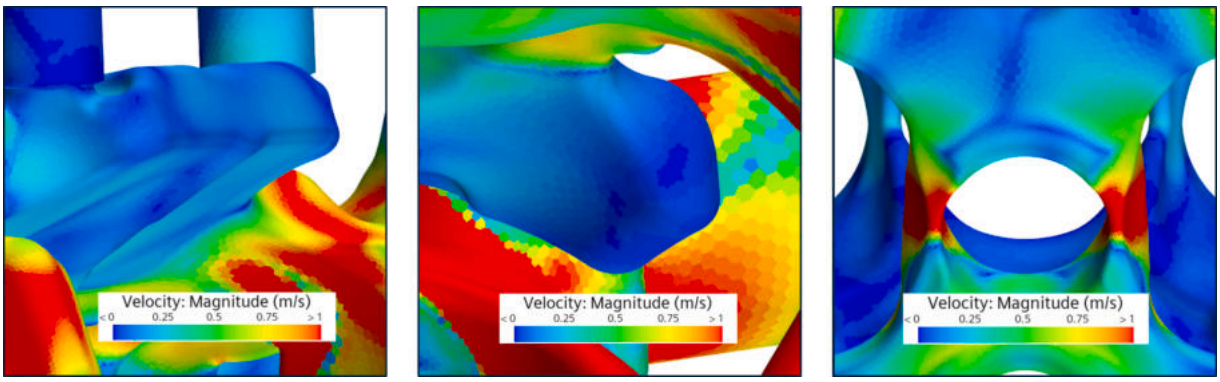

Fig. 11. Velocity magnitude in the near-wall cells of the cooling circuits, in correspondence of the regions characterized by erosion.

threshold for the same engines and operating conditions. However, it is important to point out that the distribution of each field, especially the GEP one, does not modify. In other words, it is simply scaled. This means that the capability of the GEP to identify regions of potential damage remains.

As a future development, the mechanical properties of the solid may be included in the GEP formulation. For instance, the tensile strength (effective indicator for fatigue strength, which is in turn representative for the erosion resistance) could be included in Eq. (6). In particular, it should be placed at the denominator to point out that GEP is inversely proportional to the strength. The higher the strength is, the lower GEP and erosion result. In this way, ideally, the GEP threshold would be material-independent, as the impact of the mechanical properties would be already included in the formulation. Similarly, also the effect of the time could be included in Equation (6), in order to consider that, the higher the operating time is, the greater the damage becomes. By including mechanical properties and time, the GEP would be able to predict not only the existence of potential damage conditions, but it could be directly correlated to the damage itself.

As an alternative to the modification of the GEP by including the mechanical properties, an extensive experimental investigation could be considered. By experimentally analysing different conditions and materials for long time (in order to include the time effect), it would be possible to define, for each material, a threshold value below which the cooling circuit would be able to indefinitely operate at safe conditions.

5. Conclusion

Due to the increasing specific power of modern engines, cooling circuits often experience nucleate boiling, which sometimes leads to erosion of the walls with related engine failure. Therefore, at the design stage, a methodology able to predict erosion is essential to prevent severe damage in future powertrains. Although boiling in cooling circuits is a phenomenon widely studied in literature, an erosion model has never been developed, since boiling has rarely been associated to surface damage.

The present paper proposes a CFD tool able to predict potential erosion damage, due to boiling, in cooling circuits. The tool relies on both a CHT model of the engine and a purposely developed erosion parameter. The CHT model includes all the solid components and cooling circuit. Thanks to VOF multi-phase approach and Rohsenow model, it is able to simulate wall boiling within the circuit. As for the erosion model, it does not attribute the origin of the damage to the micro-jet following the bubble collapse. Rather, the collapse of the spherical micro-bubbles forming as a consequence of the micro-jet is assumed as leading phenomenon. The micro-bubbles generate high-pressure shockwaves able to deform the material. The proposed model is synthetized by an erosion parameter (GEP) that incorporates the characteristic quantities of the boiling phenomenon, namely vapor volume fraction, liquid subcooling level, temperature gradient of the liquid and flow velocity. The higher the erosion parameter is, the higher the risk of severe damage results.

The proposed CFD tool is validated against experimental data of two different engines and multiple operating conditions. In particular, the CHT model is validated against thermocouple measurements that provide information about the engine thermal field. The error between numerical temperatures and experimental counterparts is always lower than 6 %. As for the erosion model, it is validated thanks to the experimental images showing the erosion detected in the circuits. The predicted regions of potential boiling-induced damage, indicated by the peaks of GEP distribution, prove strong correlation with the experimental images. In addition, a preliminary threshold value is identified for GEP. In fact, it is found that values higher than 5 lead to erosion for sure in the investigated engines.

Therefore, the proposed CFD tool not only enhances the understanding of the phenomenon but also provides a CFD-based methodology that can support the design and optimization of cooling circuits. Although the erosion model is developed to investigate damage in high-performance current-production reciprocating internal combustion engines, it can be applied to any engine or cooling circuit.

Declaration of competing interest

The authors declare that they have no known competing financial interests or personal relationships that could have appeared to influence the work reported in this paper.

Acknowledgments

The authors gratefully acknowledge the University of Modena and Reggio Emilia for supporting the activity by the “Fondo di Ateneo per la Ricerca 2025 per il finanziamento di piani di sviluppo dipartimentale nell’ambito della ricerca” (FARD 2025).

Appendix

The most detailed numerical approach to describe multiphase flows is the Eulerian Multiphase (EMP) one, as it is the only available method in Eulerian framework that allows to solve transport equations separately for each phase. However, the need to solve a larger number of equations at each iteration results in a higher computational cost. Additionally, the significant numerical instability associated with this approach makes the

simulation convergence particularly challenging. In this work, the EMP approach is adopted in parallel to the simpler VOF model. The goal is not to propose an alternative to VOF, because of the cost and instability issues mentioned above. Rather, it is proficiently adopted at this stage of erosion model development to validate the assumptions carried out in VOF framework for the calculation of ΔT_{sub}. In fact, since EMP is the only method able to resolve both the liquid and vapor phase thermal fields separately, it enables an accurate evaluation of both T_{liquid} and T_{vapor}. The EMP approach is adopted to investigate engine B at 7500 rpm WOT.

Before the validation of ΔT_{sub}, a comparison between EMP and VOF is carried out in terms of numerical-experimental temperature difference. Such a comparison is proposed for two reasons. Firstly, since EMP is adopted for model development in VOF framework, coherence between the results of the models is desirable. Secondly, the comparison represents an opportunity of validation for the VOF model by a more accurate method.

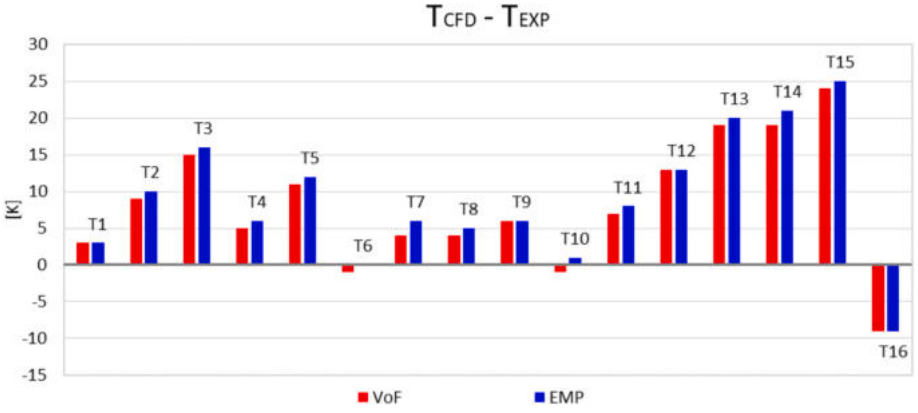

Fig. 12. Comparison between VOF and EMP approaches in terms of numerical-experimental temperature difference.

As shown in Fig. 12, the comparison between the two multiphase approaches reveals no significant difference in the computed thermal field. This result is particularly significant as it confirms the reliability of the VOF approach to accurately determine the engine thermal field. The discrepancies with the experiments can be attributed to uncertainties in the imposed boundary conditions. This is the reason why the VOF approach is proposed for the development of the CFD tool for erosion prediction, as it represents the best compromise between stability, computational cost and result quality.

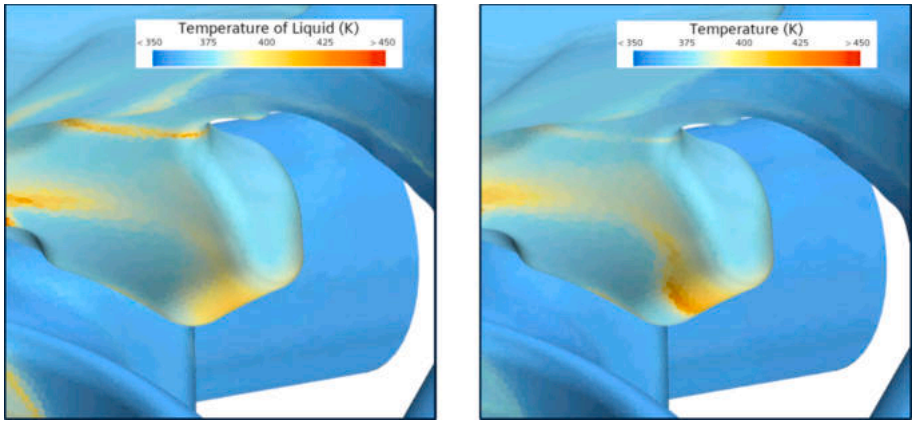

Fig. 13. Comparison between the thermal fields computed in the EMP (left) and VOF (right) approaches.

Moving to the ΔT_{sub} validation, EMP confirms that the liquid temperature can be reasonably approximated by the mixture temperature (i.e. cell temperature) available in the VOF approach, as visible by the comparison presented in Fig. 13 between the thermal field of the liquid phase and that of the liquid–vapor mixture.

Moreover, as shown in Fig. 14, the vapor phase temperature remains nearly constant at approximately 430 K, corresponding to the saturation temperature at the local circuit pressure. It is necessary to point out that, although Fig. 14 shows very different values of temperature, the region that is actually characterized by presence of vapor (the one shown in Fig. 9a)) presents values that are roughly constant and close to 430 K. In other words, Fig. 14 validates the assumption that the vapor temperature remains fixed at the saturation temperature within the region of interest. Thanks to this assumption, it is possible to estimate the vapor phase temperature even in VOF approach, once pressure field and saturation curve of the coolant are known.

Concluding, the EMP approach allows to validate the assumptions adopted within the VOF framework for the estimation of ΔT_{sub}, which is a key factor in the calculation of the erosion parameter.

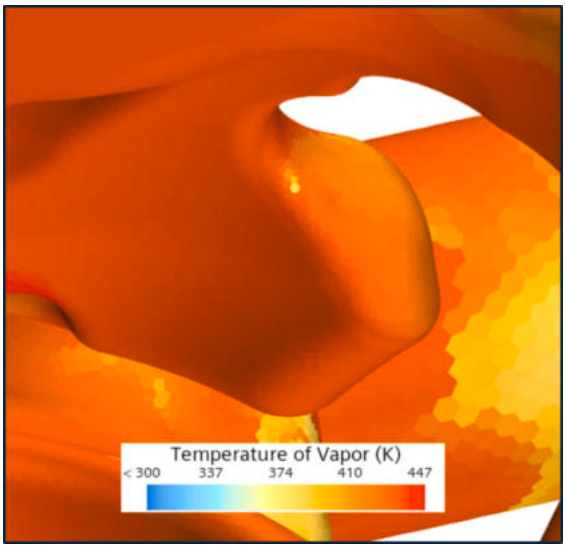

Fig. 14. Temperature of the vapor phase in the EMP approach.

Data availability

The data that has been used is confidential.

References

[1] D. Kim, J. Hwang, S. Han, C. Bae, Effects of cylinder head temperature and coolant velocity on the erosion behavior of water jacket in a diesel engine, Wear 342–343 (2015) 117–128, https://doi.org/10.1016/j.wear.2015.06.021.

[2] Ç.S. Köksal, O. Usta, B. Aktas, M. Atlar, E. Korkut, Numerical prediction of cavitation erosion to investigate the effect of wake on marine propellers, Ocean Eng. 239 (2021) 109820, https://doi.org/10.1016/j.oceaneng.2021.109820.

[3] G. Li, et al., Liquid-vapor two-phase flow in centrifugal pump: cavitation, mass transfer, and impeller structure optimization, Vacuum 201 (2022) 111102, https://doi.org/10.1016/j.vacuum.2022.111102.

[4] R. Tao, R. Xiao, F. Wang, W. Liu, Cavitation behavior study in the pump mode of a reversible pump-turbine, Renew. Energy 125 (2018) 655–667, https://doi.org/10.1016/j.renene.2018.02.114.

[5] G. Bergeles, J. Li, L. Wang, F. Koukouvinis, M. Gavaises, An Erosion Aggressiveness Index (EAI) based on pressure load estimation due to bubble collapse in cavitating flows within the RANS solvers, SAE Int. J. Engines 8 (2015) 2276–2284.

[6] S. Fontanesi, M. Giacopini, G. Cicalese, S. Sissa, S. Fantoni, Numerical investigation of the cavitation damage in the wet cylinder liner of a high performance motorbike engine, Eng. Fail. Anal. 44 (2014) 408–423, https://doi.org/10.1016/j.engfailanal.2014.05.025.

[7] M. Dular, T. Požar, J. Zevnik, R. Petkovšek, High speed observation of damage created by a collapse of a single cavitation bubble, Wear 418–419 (2019) 13–23, https://doi.org/10.1016/j.wear.2018.11.004.

[8] L. Geng, D. Zhang, J. Chen, O. De La Torre, X. Escaler, Prediction of cavitation erosion with different erosion risk indicators, Ocean Eng. 247 (2022) 110633, https://doi.org/10.1016/j.oceaneng.2022.110633.

[9] H. Wang, B. Zhu, Numerical prediction of impact force in cavitating flows, J. Fluids Eng. 132 (10) (2010) Oct, https://doi.org/10.1115/1.4002506.

[10] K. Peng, F.G.F. Qin, R. Jiang, S. Kang, Interpreting the influence of liquid temperature on cavitation collapse intensity through bubble dynamic analysis, Ultrason. Sonochem. 69 (2020), https://doi.org/10.1016/j.ultsonch.2020.105253.

[11] M. Dular, Hydrodynamic cavitation damage in water at elevated temperatures, Wear 346–347 (2016) 78–86, https://doi.org/10.1016/j.wear.2015.11.007.

[12] R.F. Patella, A. Archer, C. Flageul, Numerical and experimental investigations on cavitation erosion, IOP Conf. Ser.: Earth Environ. Sci 15 (2) (2012) 022013, https://doi.org/10.1088/1755-1315/15/2/022013.

[13] C. Leclercq, A. Archer, R. Fortes-Patella, F. Cerru, Numerical cavitation intensity on a hydrofoil for 3D homogeneous unsteady viscous flows, IJFMS 10 (3) (2017) 254–263, https://doi.org/10.5293/IJFMS.2017.10.3.254.

[14] O. Usta, E. Korkut, Prediction of cavitation development and cavitation erosion on hydrofoils and propellers by detached Eddy simulation, Ocean Eng. 191 (2019) 106512, https://doi.org/10.1016/j.oceaneng.2019.106512.

[15] M. Dular, O. Coutier-Delgosha, Numerical modelling of cavitation erosion, Int. J. Numer. Methods Fluids 61 (2009) 1388–1410, https://doi.org/10.1002/fld.2003.

[16] A. Peters, H. Sagar, U. Lantermann, O. el Moctar, Numerical modelling and prediction of cavitation erosion, Wear 338–339 (2015) 189–201, https://doi.org/10.1016/j.wear.2015.06.009.

[17] J. Tang, R. Hu, H. Liu, Z. Mo, L. Sun, Numerical investigation of thermally controlled bubble condensation near a solid wall, Chem. Eng. Sci. 262 (2022) 118018, https://doi.org/10.1016/j.ces.2022.118018.

[18] J.F. Lu, X.F. Peng, Bubble jet flow formation during boiling of subcooled water on fine wires, Int. J. Heat Mass Transf. 50 (19) (2007) 3966–3976, https://doi.org/10.1016/j.ijheatmasstransfer.2007.01.055.

[19] H. Wang, X.F. Peng, B.X. Wang, D.J. Lee, Jet flow phenomena during nucleate boiling, Int. J. Heat Mass Transf. 45 (6) (2002) 1359–1363, https://doi.org/10.1016/S0017-9310(01)00246-0.

[20] V.M. Chudnovskii, A.A. Levin, V.I. Yusupov, M.A. Guzev, A.A. Chernov, The formation of a cumulative jet during the collapse of a vapor bubble in a subcooled liquid formed as a result of laser heating, Int. J. Heat Mass Transf. 150 (2020) 119286, https://doi.org/10.1016/j.ijheatmasstransfer.2019.119286.

[21] R.V. Fursenko, V.M. Chudnovskii, S.S. Minaev, J. Okajima, Mechanism of high velocity jet formation after a gas bubble collapse near the micro fiber immersed in a liquid, Int. J. Heat Mass Transf. 163 (2020) 120420, https://doi.org/10.1016/j.ijheatmasstransfer.2020.120420.

[22] V.A. Kosyakov, R.V. Fursenko, V.M. Chudnovskii, S.S. Minaev, Physical mechanisms controlling a vapor bubble collapse and formation of a liquid jet during a laser-induced subcooled boiling near the end face of a thin waveguide, Int. Commun. Heat Mass Transfer 148 (2023) 107053, https://doi.org/10.1016/j.icheatmasstransfer.2023.107053.

[23] F. Berni, G. Cicalese, S. Fontanesi, A modified thermal wall function for the estimation of gas-to-wall heat fluxes in CFD in-cylinder simulations of high performance spark-ignition engines, Appl. Therm. Eng. 115 (2017), https://doi.org/10.1016/j.applthermaleng.2017.01.055.

[24] G. Cicalese, F. Berni, S. Fontanesi, Integrated in-cylinder / CHT methodology for the simulation of the engine thermal field: an application to high performance turbocharged DISI engines, SAE Int. J. Engines 9 (1) (2016), https://doi.org/10.4271/2016-01-0578.

[25] G. Cicalese, F. Berni, S. Fontanesi, A. D'Adamo, E. Andreoli, A Comprehensive CFD-CHT methodology for the characterization of a diesel engine: from the heat transfer prediction to the thermal field evaluation, SAE Technical Paper 2017 (2017), https://doi.org/10.4271/2017-01-2196.

[26] S. Fontanesi, M. Olcuire, G. Cicalese, L. Lamberti, F. Pulvirenti, F. Berni, Computational Fluid Dynamics (CFD) analysis of lubricant oil tank sloshing of a high-performance car under racetrack maneuvers, SAE Int J Engines 15 (2) (2022) 185–202.

[27] SIEMENS DISW, " STAR-CCM+ 17.06.008 User Guide.".

[28] W.M. Rohsenow, A method of correlating heat-transfer data for surface boiling of liquids, Trans. Am. Soc. Mech. Eng. 74 (6) (2022) 969–975, https://doi.org/10.1115/1.4015984.

[29] I.l. Pioro, Experimental evaluation of constants for the Rohsenow pool boiling correlation, Int. J. Heat Mass Transf. 42 (11) (1999) 2003–2013, https://doi.org/10.1016/S0017-9310(98)00294-4.

[30] S. Vasudevan, S. Etemad, L. Davidson, G. Montero Villar, Numerical model to estimate subcooled flow boiling heat flux and to indicate vapor bubble interaction, Int. J. Heat Mass Transf. 170 (2021) 121038, https://doi.org/10.1016/j.ijheatmasstransfer.2021.121038.

[31] F. Ramstorfer, H. Steiner, G. Brenn, Modeling of the microconvective contribution to wall heat transfer in subcooled boiling flow, Int. J. Heat Mass Transf. 51 (15) (2008) 4069–4082, https://doi.org/10.1016/j.ijheatmasstransfer.2007.10.039.

[32] F. Ramstorfer, H. Steiner, G. Brenn, C. Kormann, F. Rammer, Subcooled boiling flow heat transfer from plain and enhanced surfaces in automotive applications, J. Heat Transf. 130 (1) (2008), https://doi.org/10.1115/1.2780178.
[33] S. Vasudevan, M. Bovo, Subcooled flow boiling in high power density internal combustion engines II: numerical modeling, SAE Int. J. Engines (2023).
[34] M. Langari, et al., Conjugate heat transfer predictions for subcooled boiling flow in a horizontal channel using a volume-of-fluid framework, J. Heat Transf. 140 (10) (2018), https://doi.org/10.1115/1.4040358.
[35] V.R. Sontireddy, S. Hari, Sub cooled boiling: validation by using different CFD models, in: 2016 IEEE 23rd International Conference on High Performance Computing Workshops (HiPCW), 2016, pp. 90–99, https://doi.org/10.1109/HiPCW.2016.021.